

Time delay in QSO 0957+561 from 1984-99 optical data

A. Oscoz¹, D. Alcalde¹, M. Serra-Ricart¹, E. Mediavilla¹, C. Abajas¹, R. Barrena¹, J. Licandro¹,
V. Motta¹, and J. A. Muñoz¹

aoscoz@ll.iac.es, dalcalde@ll.iac.es, mserra@ot.iac.es, goicol@besaya.unican.es,
emg@ll.iac.es, abajas@ll.iac.es, rbarrena@ll.iac.es, jlicandr@ll.iac.es,
vmotta@ll.iac.es, jmunoz@ll.iac.es

ABSTRACT

Photometric optical data of QSO 0957+561 covering the period 1984–99 are analyzed to discern between the two values of the time delay (417 and 424 days) mostly accepted in the recent literature. The observations, performed by groups from three different institutions—Princeton University, Harvard-Smithsonian Center for Astrophysics, and Instituto de Astrofísica de Canarias—and including new unpublished 1998–9 data from the IAC80 Telescope, were obtained in five filters (V , R , I , g , and r). The different light curves have been divided into observational seasons and two restriction have been applied to better calculate the time delay: (i) points with a strange photometric behavior have been removed; and (ii) data sets without large gaps have been selected. Simulated data were generated to test several numerical methods intended to compute the time delay ($\Delta\tau_{AB}$). The methods giving the best results—the discrete correlation function, δ -square, z-transformed discrete correlation function, and linear interpolation—were then applied to real data. A first analysis of the 23 different time delays derived from each technique shows that $\Delta\tau_{AB}$ must be into the interval 420–424 days. From our statistical study, a most probable value of $\Delta\tau_{AB} = 422.6 \pm 0.6$ days is inferred.

Subject headings: quasars: individual: Q0957+561—cosmology: gravitational lensing—
photometry: DAOPHOT—methods: data analysis

1. Introduction

The first discovered gravitational lens system, QSO 0957+561 (Walsh, Carswell, & Weymann 1979), has been the subject of a continuous and exhaustive monitoring in several bands since 1979. The special characteristics of this system made it very attractive for time delay determinations, and different values for this quantity were presented during the 1980s: $\Delta\tau = 566 \pm 37$ days (Florentin-Nielsen 1984); $\Delta\tau = 376 \pm 37$ days (Schild & Cholfn 1986); $\Delta\tau = 657 \pm 73$ days (Gondhalekar et

¹Instituto de Astrofísica de Canarias, E-38205 La Laguna, Tenerife, Spain

al. 1986); $\Delta\tau = 478 \pm 73$ days (Lehár, Hewitt, & Roberts 1989). As can be seen, there was wide dispersion in the results obtained by different groups. However, the monitoring campaigns carried out during the early 1990s led to quite an odd situation, as all the results concentrate around two different values for the time delay: $\Delta\tau \sim 420$ days and $\Delta\tau \sim 510$ days. Calculations leading to the first value were presented by Vanderriest et al. (1989, $\Delta\tau = 415 \pm 20$ days); Schild (1990, $\Delta\tau = 404 \pm 10$ days); and Pelt et al. (1994, $\Delta\tau = 415 \pm 32$ days in the B band and $\Delta\tau = 409 \pm 23$ days in radio). On the other hand, a value close to 510 days was obtained by Beskin & Oknyanskij (1992, $\Delta\tau = 522 \pm 15$ days in the B band and $\Delta\tau = 515 \pm 15$ days in the r band); Roberts et al. (1991, $\Delta\tau = 515 \pm 37$ days); and Press, Rybicki, & Hewitt (1992a, $\Delta\tau = 536^{+14}_{-12}$ days in the B band; 1992b, $\Delta\tau = 540 \pm 12$ days in B +radio).

This situation abruptly changed when Kundić et al. (1995) presented their observations in the g and r bands. A sharp drop appeared in 1994 December and could be used to discern between the “long” (510 days) and the “short” (420 days) time delay, provided continuous monitoring of QSO 0957+561 was carried out in the first half of 1996. This monitoring was performed, and the long time delay was rejected (Oscoz et al. 1996; Kundić et al. 1997). The controversy regarding the time delay seemed to be finally solved. However, the results appearing in the literature since 1995 concentrate again around two values, 417 and 424 days. These results are summarized as follows: $\Delta\tau = 423 \pm 6$ days (Pelt et al. 1996); $\Delta\tau = 417 \pm 3$ days (Kundić et al. 1997); $\Delta\tau = 424 \pm 3$ days (Oscoz et al. 1997); $\Delta\tau = 425 \pm 17$ (Pijpers 1997); $\Delta\tau = 416.3 \pm 1.7$ days (Pelt et al. 1998); $\Delta\tau = 425 \pm 4$ days (Serra-Ricart et al. 1999); $\Delta\tau = 417.4$ days (Colley & Schild 2000).

This difference is irrelevant in the Hubble constant calculations, as the uncertainty introduced by the time delay is much lower than the uncertainty given by other factors (e.g., the main lens galaxy’s velocity dispersion or the lens modeling). However, the most accurate time delay should be used in the search for possible very rapid microlensing events in QSO 0957+561, and a week’s difference in $\Delta\tau$ could lead to the detection of false events or failure to detect real ones.

In this paper we have compiled photometric data of QSO 0957+561 from three different observing groups covering the period 1984–99 to obtain an estimate of the time delay by means of several statistical methods. This includes new unpublished data corresponding to the last observational campaign (1998–9) at the IAC80 Telescope. The data sets are presented in §2, while the methods for obtaining the time delay appear in §3. A first check of the goodness of these methods applied to simulated data is calculated in §4, and the best techniques are applied in §5 to real data. Finally, a discussion of our results appears in Section 6.

2. Selected data sets

Several monitoring campaigns of QSO 0957+561 in different bands have been performed since 1979. However, to obtain the time delay, only the observations obtained by groups from three different institutions will be considered here: Princeton University (hereafter PU), Harvard-Smithsonian

Center for Astrophysics (hereafter CfA), and the Instituto de Astrofísica de Canarias (hereafter IAC).

2.1. PU data

Images were obtained at the Apache Point Observatory 3.5 m telescope in the g and r bands. QSO 0957+561 was monitored during several observational campaigns, although only data corresponding to the first two seasons have been published (Kundić et al. 1995, 1997): (i) from 1994 December to 1995 May; and (ii) from late 1995 to mid 1996. The resulting data comprise 51+46 g -band points and 54+46 r -band points. The light curves were calculated via aperture photometry, and have neither large error bars nor significant gaps. Their main characteristic is the presence of a sharp drop of about 0.1 mag in the A -component in late 1994 December, very useful for time-delay calculations.

2.2. CfA data

This data set is the largest ever obtained for a gravitational lens system. It consists of 1069 brightness measurements in the R band, from late 1979 to mid 1996. The observations corresponding to the period 1979–89 were obtained at the Whipple Observatory 0.61 m telescope, while the remaining data were obtained with a 1.2 m telescope (Schild & Thomson 1995, and references therein). The reduction procedure followed a basic aperture photometry scheme (although a new automated photometry reduction code is now being applied by the authors, the results do not substantially differ from the “old” photometry). The error bars are not large, with the exception of the first five years. The main problem with this data set is the scarcity of observations during the first 1800 days (81 brightness measurements). Moreover, those points coincide with the largest error bars. So, we will consider the data from mid 1984 for time delay calculations.

2.3. IAC data

Lens monitoring was performed in four consecutive seasons (1996 February to June, 1996 October to 1997 July, 1997 October to 1998 July, and 1998 October to 1999 July) using the CCD camera of the 82 cm IAC-80 Telescope (IAC80 hereafter), sited at the IAC’s Teide Observatory (Tenerife, Canary Islands, Spain). A Thomson 1024×1024 chip was used, offering a field of nearly 7′.5. Standard VRI broad-band filters were used for the observations, corresponding fairly closely to the Landolt system (Landolt 1992). The final data set comprises 172 point in the V band, 301 points in the R band, and 112 points in the I band. Accurate photometry was obtained by simultaneously fitting a stellar two-dimensional profile on each component by means of DAOPHOT software (see details in Serra-Ricart et al. 1999). A new, completely automatic IRAF task has been

developed demonstrating, using a sample of simulated data, that the proposed method can achieve high-precision photometry. However, the errors bars obtained for IAC80 data are slightly larger than those of PU and CfA data. This could be explained by a decrease in chip sensibility due to the age of the CCD. In order to assess the reliability of our method using real data, simultaneous observations of QSO 0957+561 were undertaken on 1999 February 19 by using the IAC80 and the 2.5 m Nordic Optical Telescope (NOT hereafter) sited at the IAC’s Roque de los Muchachos Observatory (La Palma, Canary Islands, Spain). The final reduced results are presented in Figure 1 and Table 1 (photometric errors for comparison star H and D are also included). The NOT light-curve errors (a few millimagnitudes) are much lower than the IAC80 ones, and this difference could be explained in terms of the following: i) the NOT has a larger aperture than the IAC80, and ii) the NOT also has a better CCD chip. However, the good agreement between the two curves demonstrates that our reduction method works with high degree of accuracy. The photometric data are available at URL <http://www.iac.es/lent>.

3. Different methods to obtain time delay estimates

The large amount of data described in §2 adds new biases (different telescopes, filters, reduction processes, and behavior) to the inherent difficulty to analyse discrete, unevenly sampled temporary series. These facts led us to employ several statistical methods to calculate the time delay to increase the robustness of the results thus obtained. As a first step, several techniques will be checked by using simulated data: the discrete correlation function, dispersion spectra, δ^2 , δ^2 modified, linear interpolation, and the z -transformed discrete correlation function.

3.1. Discrete correlation function (DCF)

The DCF (Edelson & Krolik 1988) is a technique valid for any physical quantity that is observed to vary in time. For two discrete data trains, A_i and B_j , the formula representing their DCF is

$$DCF(\tau) = \frac{1}{M} \frac{(A_i - \bar{A})(B_j - \bar{B})}{\sqrt{(\sigma_A^2 - \epsilon_A^2)(\sigma_B^2 - \epsilon_B^2)}}, \quad (1)$$

averaging over the M pairs for which $\tau - \alpha \leq \Delta t_{ij} < \tau + \alpha$, α , ϵ_k , and σ_f being the bin semi-size, the measurement error associated with the data set k , and the standard deviation, respectively. The maximum of the DCF is identified with the time delay.

3.2. Dispersion spectra

The data model (Pelt et al. 1996) consists of two time series, $A_i = q(t_i) + \epsilon_A(t_i)$, $i = 1, \dots, N_A$, and $B_j = q(t_j - \Delta\tau_{BA}) + l(t_j) + \epsilon_B(t_j)$, $j = 1, \dots, N_B$, where $q(t)$ represents the intrinsic variability

of the quasar, $l(t)$ accounts for the difference in magnitudes plus additional variability in time due to microlensing, and $\epsilon_A(t)$ and $\epsilon_B(t)$ are observational errors. This two series are combined into one, C , for every fixed combination $[\tau, l(t)]$ by taking all values of A as they are and correcting the B data by $l(t)$ and shifting them by τ . The dispersion spectra that will be used here are represented by

$$D_{4,k}^2 = \min_{l(t)} \frac{\sum_{n=1}^{N-1} \sum_{m=n+1}^N S_{n,m}^{(k)} W_{n,m} G_{n,m} (C_n - C_m)^2}{\sum_{n=1}^{N-1} \sum_{m=n+1}^N S_{n,m}^{(k)} W_{n,m} G_{n,m}}, \quad (2)$$

where the $W_{n,m}$ are statistical weights of the combined light curves, and $G_{n,m} = 1$ when C_n and C_m come from different curves (A or B) and 0 otherwise. From eq. (2), we can consider two different approximations depending on the definition of $S_{n,m}^{(k)}$: (i) $S_{n,m}^{(1)} = 1$ if $|t_n - t_m| \leq \delta$ and 0 otherwise; and (ii) $S_{n,m}^{(2)} = 1 - |t_n - t_m|/\delta$ if $|t_n - t_m| \leq \delta$ and 0 otherwise, δ being the maximum distance between two observations which can be considered as nearby. The minimum value of eq. (2) is assumed as the time delay.

3.3. δ -square

The δ^2 method (Serra-Ricart et al. 1999) makes use of the similarity between the discrete autocorrelation function (DAC) of the light curve of one of the components and the A – B discrete correlation function (DCF). From the DAC and DCF functions, one can define a function

$$\delta_m^2(\theta) = \left(\frac{1}{N}\right) \sum_{i=1}^N S_i [\text{DCF}(\tau_i) - \text{DAC}(\tau_i - \theta)]^2 \quad (3)$$

for every fixed value θ (days), where $S_i = 1$ when both the DCF and DAC are defined at τ_i and $\tau_i - \theta$, respectively, and 0 otherwise. The most probable value for the time delay should correspond to the minimum of this function.

3.4. δ^2 modified

This modification of the δ^2 method was suggested by Schild (1999, private communication). It consists in comparing the DAC and DCF curves by taking their ratio instead of by calculating their difference. So, the final equation to obtain the time delay is

$$\delta_m^2(\theta) = \left(\frac{1}{N}\right) \sum_{i=1}^N S_i \left[\frac{\text{DCF}(\tau_i)}{\text{DAC}(\tau_i - \theta)} \right]^2. \quad (4)$$

3.5. Linear interpolation (LI)

The linear method is similar to that suggested by Kundić et al. (1997). One of the two light curves (hereafter light curve 1) is selected, and the linear interpolation of data and their errors is considered as reference. The other light curve (hereafter light curve 2) is then shifted in magnitude by just the difference between the means of both light curves. After that, light curve 2 is shifted in time and chi-square per degree of freedom ($\bar{\chi}^2$) for each time delay is calculated. The number of degrees of freedom is equal to the number of points of the light curve 2 in the overlapping interval minus 2 (because we are fitting shifts in magnitude and time). The time that minimizes $\bar{\chi}^2$ is taken as a provisional time delay.

This procedure is followed by using as reference both the *A*- and *B*-component light curves, selecting then the time delay closest to 421 days (the intermediate point between 417 and 425 days). The uneven sampling of the light curves usually leads to a better time delay taking as a reference one of the two light curves.

3.6. *z*-transformed discrete correlation function (ZDCF)

The ZDCF (Alexander 1997) is a new method for estimating the cross-correlation function (CCF) of sparse, unevenly sampled light curves. Fisher’s *z*-transform of the linear correlation coefficient, *r*, is used to estimate the confidence level of a measured correlation. This technique attempts to correct the biases that affect the original DCF by using equal-population binning. The ZDCF involves three steps:

- (i) All possible pairs of observations, $\{a_i, b_j\}$, are sorted according to their time-lag, $t_i - t_j$, and binned into equal population bins of at least 11 pairs. Multiple occurrences of the same point in a bin are discarded so that each point appears only once per bin.
- (ii) Each bin is assigned its mean time-lag and the intervals above and below the mean that contain 1σ of the points each.
- (iii) The correlation coefficients of the bins are calculated and *z*-transformed. The error is calculated in *z*-space and transformed back to *r*-space.

The time-lag corresponding to the maximum value of the ZDF is assumed as the time delay between both components.

4. Analysis of the different methods by using simulated light curves

The application of the statistical methods described in §3 to simulated data sets can serve to check the validity of their results under different conditions, always with discrete and irregularly sampled data sets. The six selected data sets are quite similar to those presented in Serra-Ricart et

al. (1999), where several sets of simulated photometric data with similar irregularity in the observations (time distribution of the data), magnitudes, and error bars (i.e., as large as or even larger than those of PU, CfA, and IAC; the worst situation is selected) to that of the IAC observations were created.

First, a set of dates, x_i , between 1800 and 2000 (TJD = JD–2449000) approximately, was generated with a pseudo-random separation, taken from a uniform distribution between 0 and 5 days. These data were alternatively separated in two time series, corresponding to A - and B -component light curves, this last curve being shifted by 420 days to simulate the existence of a time delay. A first magnitude was calculated for each date with the relationship $y_i = F(x_i)$ [see below for the different shapes of $F(x_i)$]. The probability of measuring a value y for each x_i is proportional to $e^{[-(y-y_i)^2/2\sigma_i^2]}$, and hence characterized by σ_i , or, equivalently, the variable $d = y - y_i$ is distributed as $e^{[-d^2/2\sigma_i^2]}$. A σ_i taking pseudo-random values between 0.01 and 0.03 was generated for each x_i . From here the quantities d_i , pseudo-random numbers obtained from a normal Gaussian distribution with zero mean and standard deviation, σ_i , were calculated, allowing them to adopt positive or negative values. Finally, the magnitude was generated from the equation $y_o = F(x_i) + d_i = y_i + d_i$, with an error bar of σ_i . The A component was made brighter by adding 0.1 to the magnitudes of the B component.

The first selected function was:

$$F1 : y = 17.17 + 0.5 e^{-0.5f} \sin(f), \quad \text{where } f = \frac{(x - 1800)}{20}. \quad (5)$$

This function represents light curves in which a sharp event similar to that reported by Kundić et al. (1995) appears.

The second function is

$$F2 : y = 17.2 + 0.1 \sin(f) \sin(4f), \quad \text{where } f = \frac{x}{40}. \quad (6)$$

In this case, the light curves present several maxima and minima, although none of them is clearly remarkable.

An additional function, consistent with the actual variability of Q0957+561, was created (the IAC observational data from 97–98 seasons, were selected as reference). The light curves were then fitted by the function

$$F3 : y = 17.07 - 0.16 e^f, \quad \text{where } f = \frac{-(x - 15.8 - m)^2}{2(10 + s)^2}, \quad (7)$$

m being the mean of the TJD in the selected range and s its standard deviation. The resulting simulated data show a lower variability to that obtained from $F1$ and $F2$.

Besides the comparison between the A - and B -component for the three data sets, an additional test was performed by removing some data of the A -component. By doing this, we want to simulate

the data sets corresponding to certain periods in which no valid data could be obtained during several days (bad weather, problems with the telescope, etc.).

The time delay corresponding to the different statistical techniques were first calculated by allowing their free parameters to vary. The best results were obtained with a $\alpha = 5$ days for the DCF, $\alpha = 2$ days for $D_{4,1}^2$ and $D_{4,2}^2$, and $\delta = 10$ days for δ^2 and δ_m^2 . In the DCF, δ^2 and δ_m^2 cases, the results were quite similar for the parameters varying between 4 and 12 days. However, slightly better values were obtained for $\alpha = 5$ days in the DCF case, and for $\delta = 10$ days in the δ^2 and δ_m^2 cases, so these quantities were selected. The objective in this paper is to analyze the different methods with several data sets by using the same conditions. An analysis of the best method and/or parameters to be used with a particular data set will be presented in a future paper. The uncertainties in the time-delay estimates were computed by generating 1000 bootstrap samples and applying the statistical methods in each case.

Some interesting consequences can be derived from the results in Table 2. As expected, the best estimate of the time delay is always obtained for the function $F1$, i.e., when a sharp drop similar to the one appearing in §2.1 is present in the light curves. All the methods give a good value for the delay. On the other hand, in the $F2$ and $F3$ cases the error bars are too large for δ_m^2 , $D_{4,1}^2$, and $D_{4,2}^2$ when compared with the results obtained with the other methods. So only the DCF, δ^2 , ZDCF, and LI techniques will be applied to real data calculations, similar in most of the cases to the functions $F2$ and $F3$. Notice that the true time delay is always within the error bar, even when a large gap is present in the light curves.

5. Time delay from real data

Prior to applying the different methods to calculate the time delay from real data, some considerations have to be taken into account. First, data should be checked to eliminate inconsistent measurements. This modification of the raw data, based on a suggestion by Falco (1997, private communication), takes account of the possible existence of strong and simultaneous (not time-shifted) variations of some data point in both components. The inclusion of such “strange” brightness records in the final data sets probably originated from failures in the CCD or from bad weather conditions, creates artificial peaks or valleys in the light curve of one of the components. These maxima/minima have no importance when a sharp change in the behavior of the quasar is being analyzed, but can lead to a completely wrong time delay estimate when dealing with a smoother season. To avoid these abnormal observations we have removed the points with a simultaneous difference in magnitude in both components as compared with the previous and following records larger than 2.5 times their error bar. This was done by considering only those points with a difference in the observation dates of less than 10 days. The resulting data sets will be named bad point free (BPF). The 301 points of the IAC data set in the R band are reduced to 289 with this restriction, while less than 60 of the 1069 CfA observations have to be removed. Finally, no brightness measurement of the PU data seems to be wrong. However, the BPF restriction could be

applied neither to the IAC I - and V -band data nor to the CfA 89–90 and 91–92 R -band data due to their low number of points, with a minimum distance between neighboring points more than 10 days in most of the cases.

Another drawback when dealing with real data is the impossibility of observing the system during certain months of the year and the consequent lack of suitable edges. Once it is stated, see §1, that the rough value of the time delay is around 420 days, the comparison between the A and B components should be made by previously selecting a “clean” data set (CD, see Serra-Ricart et al. 1999), i.e., homogeneous monitoring of both images during two active and clear (free from large gaps) epochs separated by ~ 420 days.

Finally, both types of corrections, BPF and CD, were combined to obtain the definitive data sets used in this paper. To see the importance of applying the CD–BPF corrections, we mention two extreme examples: 1) $\Delta\tau = 398 \pm 11$ days with the raw IAC data corresponding to the 96–7 season, while $\Delta\tau = 428 \pm 9$ days with the CD–BPF approximation; and (2) $\Delta\tau = 384 \pm 5$ days with the original 93–4 CfA data and $\Delta\tau = 423 \pm 2$ days with the CD–BPF approximation.

To summarize, Monte Carlo calculations were applied to the four techniques (DCF, δ^2 , ZDCF, and LI) with the CD and the CD-BPF restrictions. The PU, IAC, and CfA data sets were divided into observational seasons, leading to the 23 different time-delay estimates per method appearing in Tables 3 to 6. The results obtained from the PU data in both the g and r filter are presented in Table 3. Notice that two of the methods (DCF and LI) employed here are also used by Kundić et al. (1997). Our results are quite similar to those obtained by these authors, and, moreover, they are always into their error. The small differences come from the selection of clean data sets. Tables 4 and 5 offer the time delay for the IAC data in the R , and in the I and V bands, respectively. Finally, Table 6 was obtained from the CfA R band data. The analysis of these delays are done by considering the CD–BPF quantities, except in those cases in which only the CD results could be obtained. The quantities obtained for the CfA 92–3 season with the DCF and δ^2 methods can be discarded, as they appear to be clearly inconsistent (394 ± 1 and 403 ± 1 days, respectively).

6. Discussion and conclusions

A first step in discussing the value of $\Delta\tau_{AB}$ consists in computing, for each of the techniques (DCF, δ^2 , ZDCF, and LI), the number of occurrences of each value of the time delay. These quantities, obtained from Tables 3 to 6, are depicted by the black lines in Figure 2: DCF (top panel, left); δ^2 (top panel, right); ZDCF (bottom panel, left); and LI (bottom panel, right). (The different values of $\Delta\tau_{AB}$ have been grouped into two-day bins). As can be seen, two remarkable characteristics can be deduced from Figure 2: (i) there is a small dispersion in the delays, as most of them are in the interval 415–428 days; and (ii) the centroids of the histograms, given by the average of the time delays derived in Tables 3 to 6, are always in the interval 420–424 days. These last quantities are represented in Figure 2 (open circles) together with their uncertainty (r.m.s., see

Table 7 and discussion below). Note that the largest peak of each histogram coincides with this average value, except for the ZDCF technique. In the histogram corresponding to δ^2 , the maximum corresponds to the values 421–424, while the average is 421.8 ± 1.3 days. The DCF panel does not lead to a clear time delay, with two maxima in the intervals 417–420 and 423–424 days. The average here is given by 423.3 ± 1.4 days. In the case of LI, the peak is placed at $\Delta\tau_{AB} = 423$ –424 days, and the average is 424.3 ± 1.2 days. Finally, the ZDCF method has a maximum around 423–424 days. However, the average is 420.6 ± 1.1 days, which is slightly different. The red histograms in Figure 2 represent the total number of occurrences obtained by adding the results from the four techniques. Its center is again over 420 days, giving a maximum of 423–424 days.

To complement these calculations, which have been done by fixing the method and computing the probability of appearance of each delay, we can now represent the number of times each value appears for each data set, independently of the method employed. Four different data sets have been selected: (i) PU r and g filters, Figure 3a; (ii) IAC R data, Figure 3b; (iii) IAC V and I records, Figure 3c; and (iv) CfA R data, Figure 3d. In this case, the centroid of the distributions, represented by open circles in Figure 3, is again over 420 days: 421.4 ± 1.1 days, 423.7 ± 1.3 days, 423.7 ± 1.2 days, and 421.8 ± 1.0 , for PU r and g , IAC R , IAC I and V , and CfA R , respectively. A first positive consequence of the PU results is their extremely short dispersion indicating the goodness of the data and the presence of the sharp event. The maximum here is placed between 419 and 424 days. However, the clearest peak appears from the IAC R values around 423–424 days. The IAC I and V panel shows more dispersion, probably due to the higher error bars of the light curves. There is not a unique maximum here, as two peaks appear around 423–424 and 427–428 days. The highest dispersion in the results can be seen in Figure 3d, corresponding to the CfA data. The maximum would in this case be in the interval 417–422 days. A remarkable result here is that the average coincides with the maxima in all the panels. Once again, the red histogram gives the total number of occurrences.

The combination of the results derived from Figures 2 and 3 (centroids and maxima of the distributions) support a $\Delta\tau_{AB}$ in the range of 420–424 days, although a time delay of around 417 days cannot be totally discarded. It is important to remark that the results are the same independently of the technique employed or of the data set selected.

The time delay between A and B components of Q0957+561 does not depend on the filter (as it is an acromatic effect) and/or the time (different campaigns), so it should be possible to merge the different sample results. A very important point is to assess the statistical reliability of the different delay calculation methods in order to estimate final delay errors. Several statistics were calculated, Mean Delay ($MD = \sum_{i=1}^N \Delta\tau_{ABi}/N$), Mean Error ($ME = \sum_{i=1}^N \epsilon_i/N$, with ϵ_i individual errors), and Dispersion ($DI = [\sum_{i=1}^N (\Delta\tau_{ABi} - MD)^2/(N - 1)]^{1/2}$). If the error estimate is correct, then $ME \approx DI$, and the final error for the time delay will be given by the r.m.s. ($[\sum_{i=1}^N (\Delta\tau_{ABi} - MD)^2/(N * (N - 1))]^{1/2}$) (see Eadie et al. 1971). Tables 7 to 10 (see below) show the final results for the four methods. In all cases, within the statistical errors, good agreement is found between the mean error and the dispersion.

When this procedure is applied to the different time delays given by each technique, one obtains the results in the first four rows of Table 7, where the mean values of the time delay and the uncertainties (r.m.s.) are shown. According to these calculations, the definitive time delay would be in the interval 420(ZDCF)–424(LI) days, with an uncertainty below 1.4 days. This interval coincides with that derived from the analysis of Figures 2 and 3. When this calculation is done with only the R band results (Table 8), the results are almost identical.

The different analyses performed until now have been done considering all the results obtained in Tables 3 to 6. However, the error bars of some of these values exclude the interval 420–424 days, where, as shown before, there is the highest probability of finding the right $\Delta\tau_{AB}$. The mean delays and uncertainties obtained when these values are removed (first four rows of Table 9) are very similar to those of Table 7. $\Delta\tau_{AB}$ is now restricted to the interval 420.8–423.2 days, with an uncertainty below 1.3 days. Once again, the results derived from the R -filter data are almost the same (Table 10).

The validity of these statistical results led us to repeat the calculations of Tables 7 to 10, but this time having into account all the delays, i.e., without considering the method (DCF, δ^2 , ZDCF, or LI). This allows us to have four different time delays per year in most of the occasions, and so, a larger amount of data for the statistical analysis. The results appear in the last row of Tables 7 to 10, although only the values of Tables 7 and 9, $\Delta\tau_{AB} = 422.6 \pm 0.6$ days and $\Delta\tau_{AB} = 422.0 \pm 0.6$ days, respectively, will be considered, as they were obtained from a larger amount of data. Adopting a conservative point of view, we will select the quantity with the higher uncertainty, $\Delta\tau_{AB} = 422.6 \pm 0.6$ days, as the final time delay.

Different treatments of the time delays obtained in §5 have been performed. The analysis of these results always points to a time delay in the interval 420–424 days. None of these methods clearly favors the values 416–418 days as the right time delay. Moreover, the averages of the quantities of Tables 7 and 9 give values around 422 days, coinciding with the maxima obtained in Figures 2 and 3. Assuming this value as the time delay between the A and B components of Q0957+561, let us check which of the results given in Tables 3 to 6 include 422 days in their the error bars. Figure 4 offers the number of times, written as a percentage of the total number of time delays obtained for each method, that each value of $\Delta\tau_{AB}$ is included in these error bars. This probability is the same, 86%, for DCF, δ^2 and ZDCF, and 74% for LI. In this case, the DCF and δ^2 methods show the highest probability for a $\Delta\tau_{AB}$ of 421–422 days, while the peak in the LI curve is placed at 423 days. A wider maximum is obtained in the case of ZDCF, with the same probability between 418 and 421 days.

As can be seen, not all the seasons in the different data sets are fully appropriate for calculating the time delay. However, our intention was to analyze all the data in the three different data sets with four different methods, and finally to restrict the uncertainty in the calculation of the time delay. The statistical treatment of all the results confirms a time delay of ≈ 422 days.

We are especially grateful to E. E. Falco for advising us on the possible presence of strange points in our data sets, to R. Schild for helpful comments on the statistical methods, and to T. Alexander for providing us with his programs to calculate the ZDCF method and his help in understanding it. This work was supported by the P6-88 project of the Instituto de Astrofísica de Canarias (IAC), Universidad de Cantabria funds, and DGEIC (Spain) grant PB97-0220-C02.

REFERENCES

- Alexander, T. 1997, *Astronomical Time Series*, Maoz, D., Sternberg, A., and Leibowitz, E. M. (eds), Dordrecht: Kluwer, 163
- Beskin, G. M., and Oknyanskij, V. L. 1992, *Lecture Notes in Physics 406, Gravitational Lenses*, Kayzer, R., Schramm, T., and Refsdal S. (eds), Springer-Verlag: Heidelberg, 67
- Colley, W. N., and Schild, R. E. 2000, *ApJ*, 540, 104
- Eadie, W. T., Drijard, D., James, F. E., and Roos, M. 1971, *Statistical Methods in Experimental Physics* (Amsterdam: North-Holland)
- Edelson, R. A., and Krolik, J. H. 1988, *ApJ*, 333, 646
- Florentin-Nielsen, R. 1984, *A&A*, 138, 119
- Gondhalekar, P. M., Wilson, R., Dupree, A. K., and Burke, B.F. 1986, *London Conference Proceedings, New Insights in Astrophysics: Eight Years of Astronomy with IUE*, SP-263, 715
- Kundić, T., Colley, W. N., Gott III, J. R., Malhotra, S., Pen, U., Rhoads, J. E., Stanek, K. Z., Turner, E. L., and Wambsganss, J. 1995, *ApJ*, 455, L5
- Kundić, T., Turner, E. L., Colley, W. N., Gott III, J. R., Rhoads, J. E., Wang, Y., Bergeron, L. E., Gloria, K. A., Long, D. C, Malhotra, S., and Wambsganss, J. 1997, *ApJ*, 482, 75
- Landolt, A. U. 1992, *AJ*, 104, 340
- Lehár, J., Hewitt, J. N., and Roberts, D. H. 1989, *Gravitational Lenses*, Moran, J. M., Hewitt, J. N., and Lo, K. Y. (eds), *Gravitational Lenses*, Dordrecht: Reidel, 84
- Oscos, A., Serra-Ricart, M., Goicoechea, L. J., Buitrago J., and Mediavilla E. 1996, *ApJ*, 470, L19
- Oscos, A., Mediavilla, E., Goicoechea, L. J., Serra-Ricart, M., and Buitrago, J. 1997, *ApJ*, 479, L89
- Pelt, J., Hoff, W., Kayser, R., Refsdal, S., and Schramm, T. 1994, *A&A*, 256, 775
- Pelt, J., Kayser, R., Refsdal, S., and Schramm, T. 1996, *A&A*, 305, 97
- Pelt, J., Schild, R., Refsdal, S., and Stabell, R. 1998, *A&A*, 336, 829
- Pijpers, F. P. 1997, *MNRAS*, 289, 933
- Press, W. H., Rybicki, G. B., and Hewitt, J. N. 1992a, *ApJ*, 385, 404
- Press, W. H., Rybicki, G. B., and Hewitt, J. N. 1992b, *ApJ*, 385, 416
- Roberts, D. H., Lehár, J., Hewitt, J. N., and Burke, B. F. 1991, *Nature*, 352, 43

Schild, R. 1990, *ApJ*, 100, 1771

Schild, R. E., and Cholfin, B. 1986, *ApJ*, 300, 209

Schild, R., and Thomson, D. J. 1995, *AJ*, 109, 1970

Serra-Ricart, M., Oscoz A., Sanchís, T., Mediavilla, E., Goicoechea, L. J., Licandro, J., Alcalde, D., and Gil-Merino, R. 1999, *ApJ*, 526, 40

Vanderriest, C., Schneider, J., Herpe, G., Chevreton, M., Moles, M., and Wlérick, F. 1989, *A&A*, 215, 1

Walsh, D., Carswell, R. F., and Weymann, R. J. 1979, *Nature*, 279, 381

Fig. 1.— Light curves for *A* and *B* images of QSO 0957+561 in the *R* band obtained on the night of 1999 February 19. IAC'80 data are represented by boxes and NOT data are indicated by circles. One-sigma error bars are indicated. See text for more details.

Fig. 2.— Number of times (black lines) that each value of the time delay appears, obtained from the results of Tables 3 to 6. The four different techniques have been considered: a) DCF, b) δ^2 , c) ZDCF, d) LI. The open circles represent the average value of the delays for each method, and the red histograms represent the sum of the values given by each method.

Fig. 3.— Number of times (black lines) that each value of the time delay appears for each data set from the values given in Tables 3 to 6. Four data sets are represented: a) PU *r* and *g*, b) IAC *R*, c) IAC *I* and *V*, and d) CfA *R*. The open circles represent the average value of the delays for each data set, and the red histograms represent the total sum of the values.

Fig. 4.— Percentage of times that a value of the time delay is included in the error bars of the results given in Tables 3 to 6: black = DCF, red = δ^2 , green = ZDCF, and blue = LI.

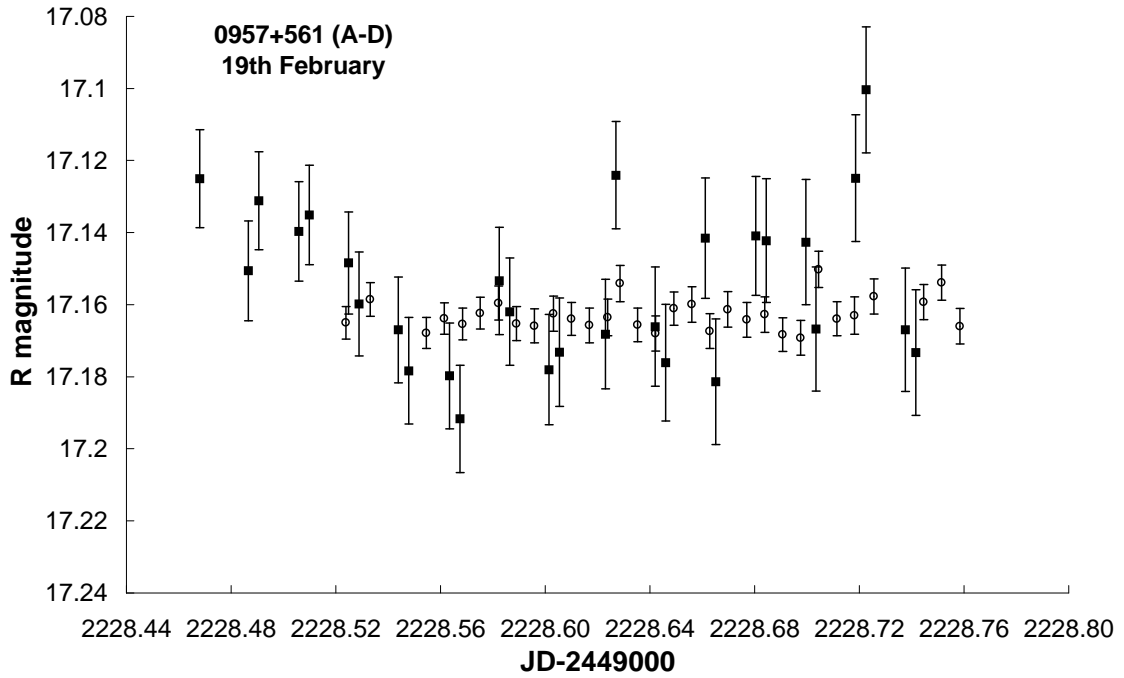
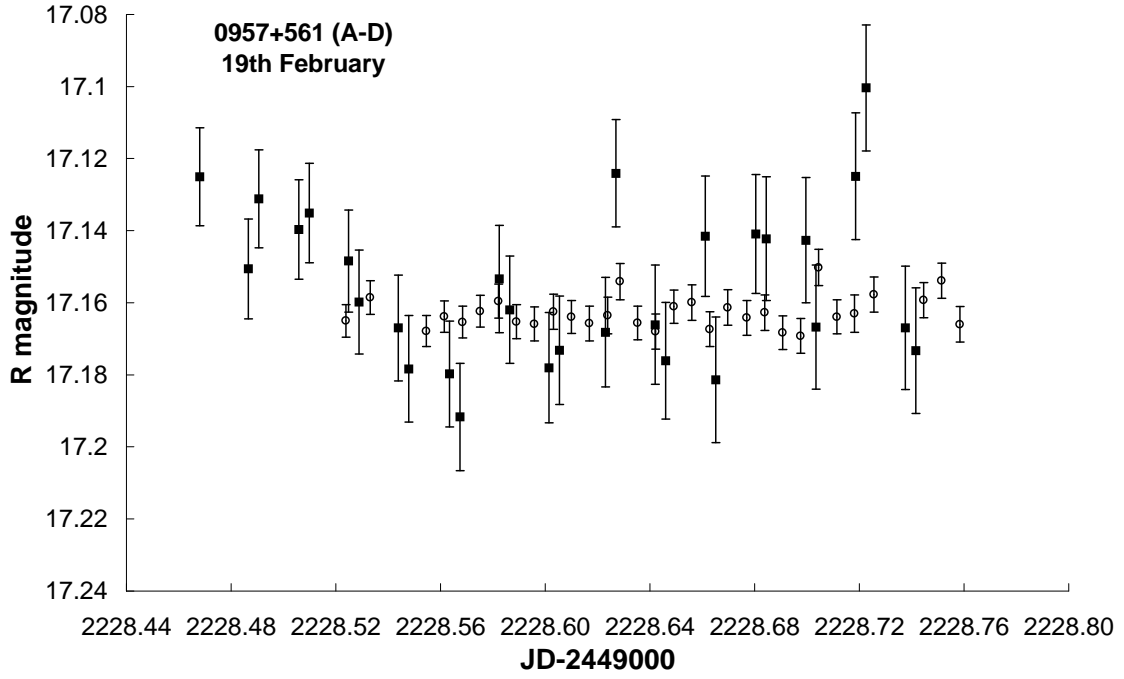


Fig. 1

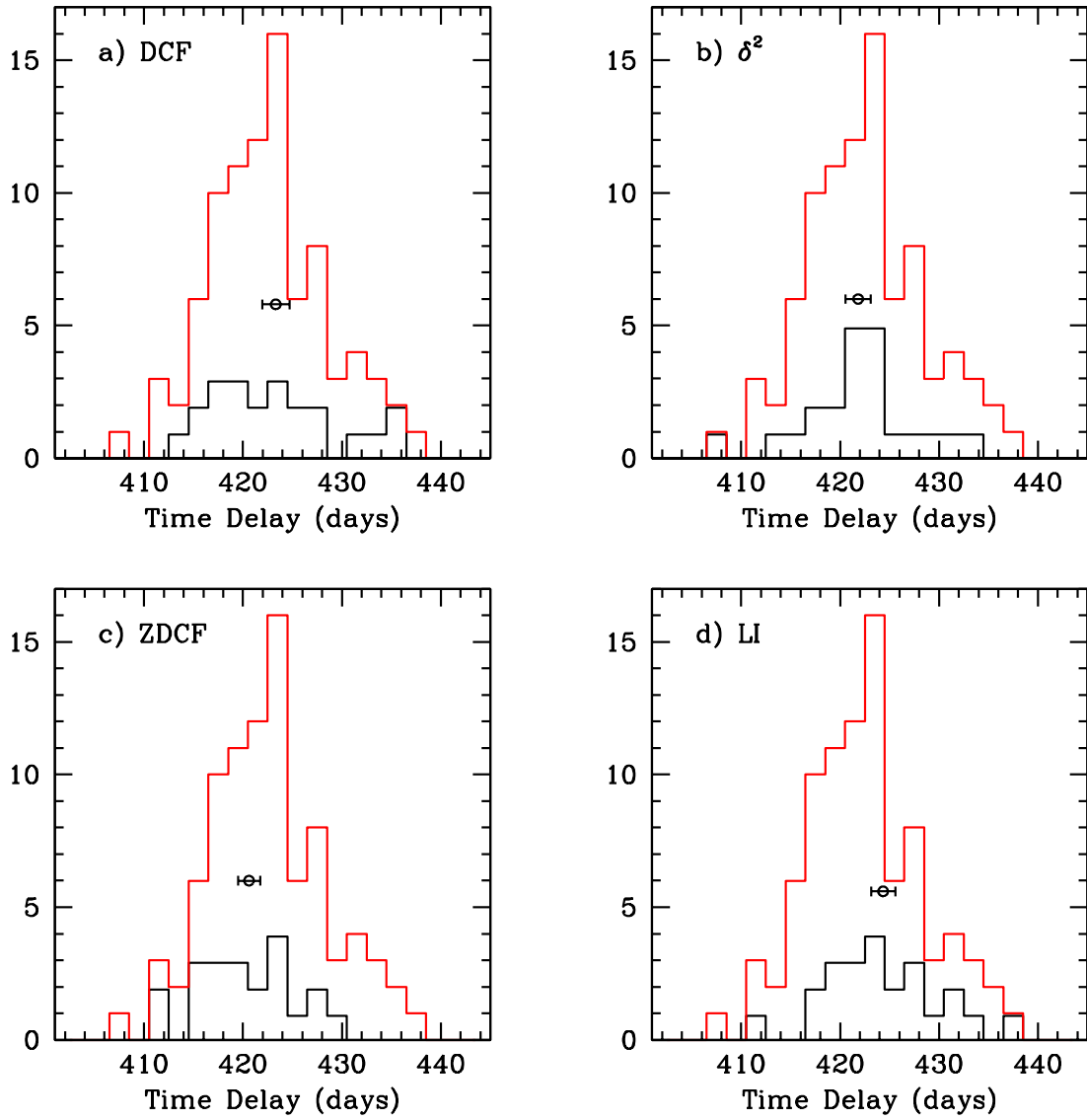


Fig. 2

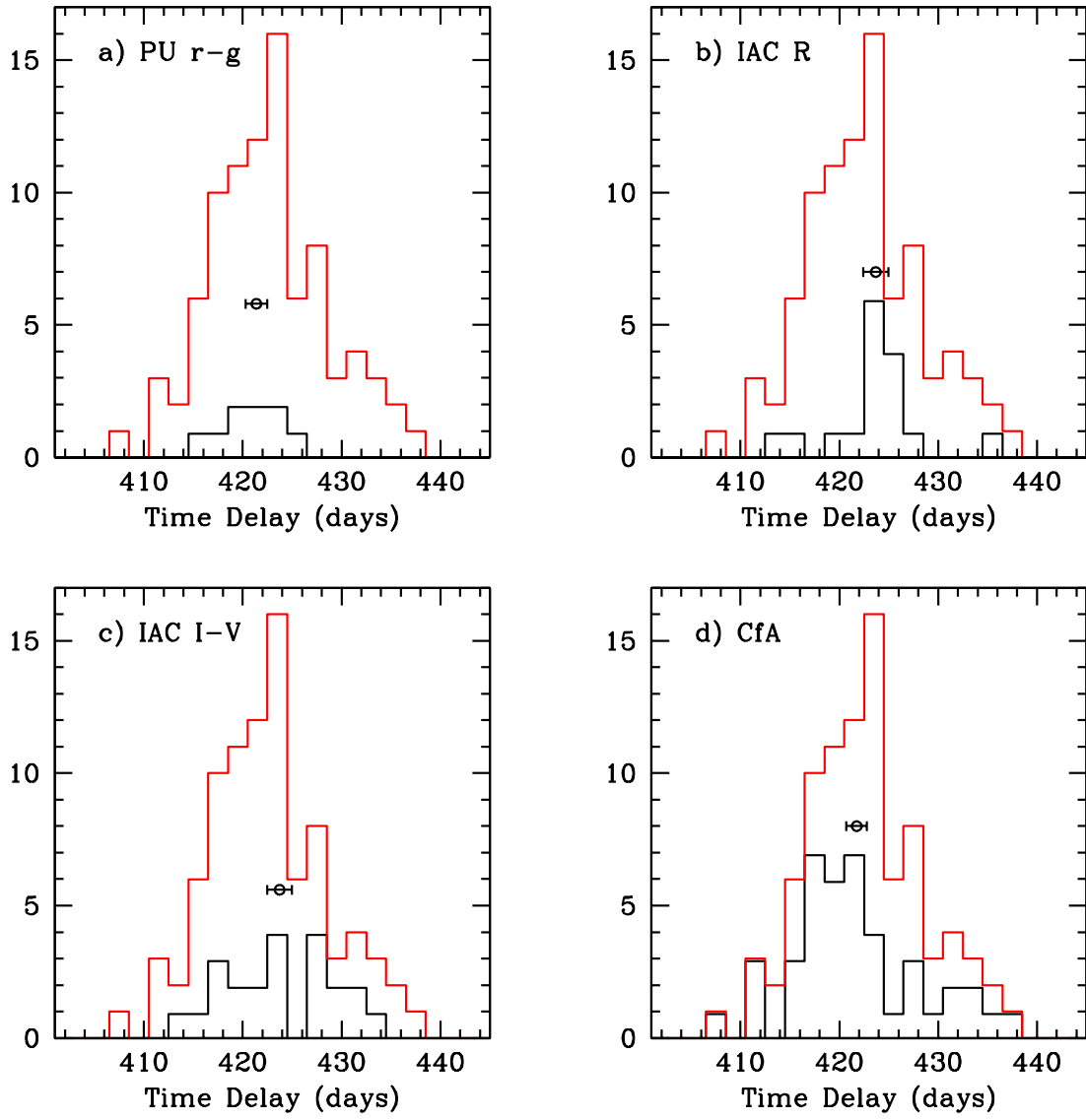


Fig. 3

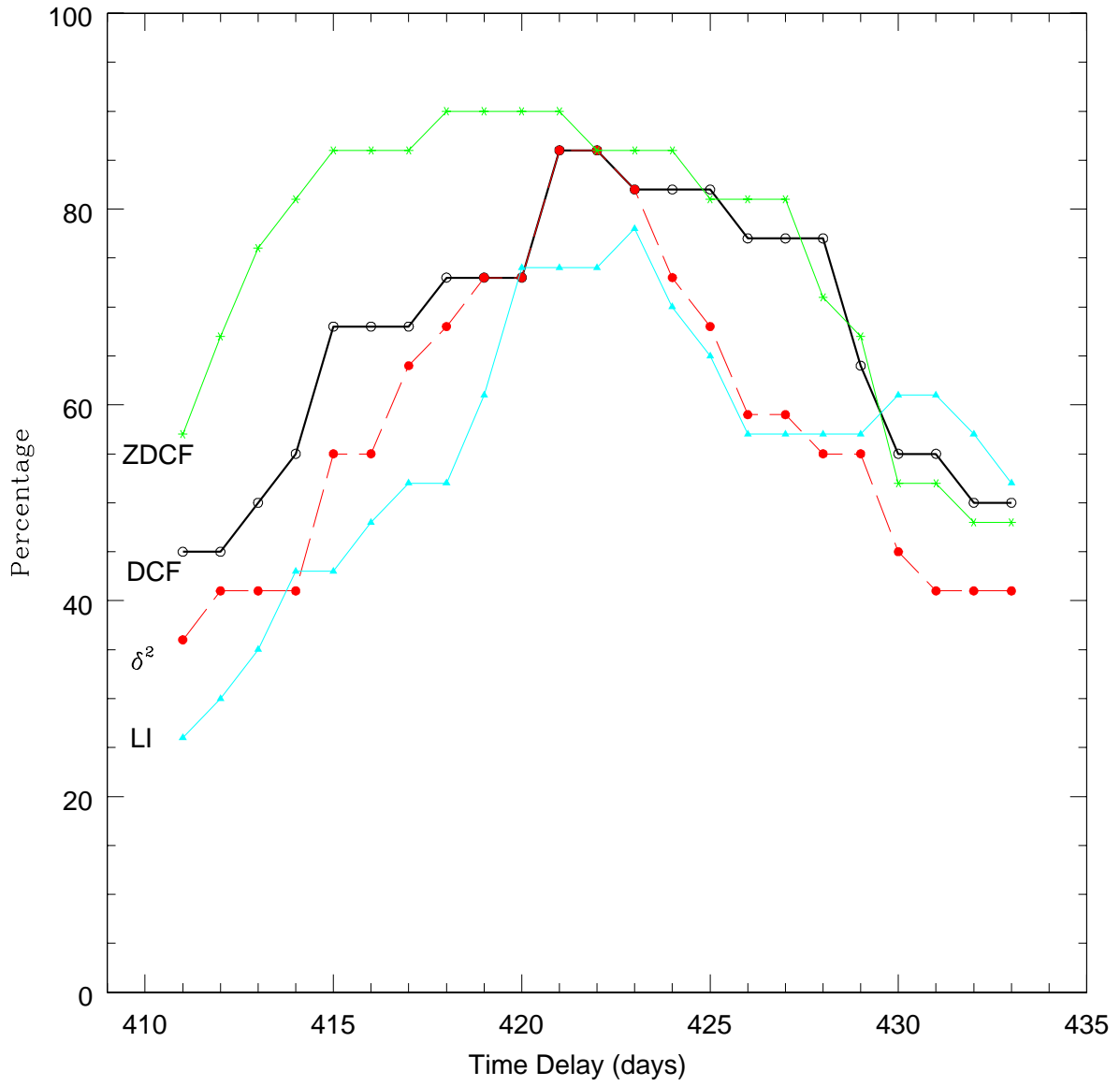


Fig. 4

Table 1. R photometric errors

Light curve ^a	NOT ^b	IAC80
A	0.005	0.016
B	0.005	0.014
H-D	0.002	0.005

^aSee section 1 for details.

^bError values are expressed in magnitudes.

Table 2: “Time delays” obtained from the application of a Monte Carlo algorithm with the different techniques to the six simulated data sets (see main text for details). The “true” time delay was 420 days.

Method	$F1$	$F1$ (gap in A)	$F2$	$F2$ (gap in A)	$F3$	$F3$ (gap in A)
DCF ($\alpha = 5$)	421±2	421±4	419±1	420±2	415±9	412±9
δ^2 ($\delta = 10$)	422±2	421±2	419±1	420±1	420±5	417±5
ZDCF	420±3	420±3	421±1	420±7	418±14	416±13
LI	421±2	421±2	420±1	421±1	419±12	418±13
δ_m^2 ($\delta = 10$)	422±9	422±13	425±30	416±34	403±34	413±29
$D_{4,1}^2$ ($\alpha = 2$)	421±3	421±4	421±12	416±20	422±27	414±25
$D_{4,2}^2$ ($\alpha = 2$)	421±2	421±3	423±15	415±26	420±26	412±21

Table 3. Time delays obtained from the application of a Monte Carlo algorithm with four different methods to the PU r and g data

Filter	Years	Method	Points (CD)	Delay (CD)
g	A (94-5); B (95-6)	DCF		422±1
		δ^2	42; 39	423±1
		ZDCF		416±2
		LI		419±5
r	A (94-5); B (95-6)	DCF		426±5
		δ^2	41; 41	423±2
		ZDCF		420±8
		LI		422±3

Table 4. Time delays obtained from the application of a Monte Carlo algorithm with four different methods to the IAC R data

Years	Method	Points (CD)	Delay (CD)	Points (CD-BPF)	Delay (CD-BPF)
A (96–8); B (97–9)	DCF		428±12		425±11
	δ^2	182; 220	421±5	173; 212	421±4
	ZDCF		418±13		426±13
	LI		421±16		424±17
A (96); B (96–7)	DCF		432±8		436±8
	δ^2	31; 36	425±8	28; 33	428±9
	ZDCF		422±13		424±14
	LI		424±7		424±7
A (96–7); B (97–8)	DCF		436±10		424±13
	δ^2	46; 86	431±4	45; 84	425±4
	ZDCF		429±13		424±12
	LI		415±16		426±16
A (97–8); B (98–9)	DCF		414±12		416±12
	δ^2	79; 62	414±10	78; 61	413±8
	ZDCF		420±12		420±13
	LI		427±13		423±13

Table 5. Time delays obtained from the application of a Monte Carlo algorithm with four different methods to the IAC I and V data

Filter	Years	Method	Points (CD)	Delay (CD)
I	A (96–8); B (97–9)	DCF		415±13
		δ^2	65; 87	423±12
		ZDCF		417±14
		LI		419±9
I	A (96); B (96–7)	DCF		424±16
		δ^2	19; 18	424±16
		ZDCF		
		LI		430±3
I	A (96–7); B (97–8)	DCF		419±9
		δ^2	18; 31	422±7
		ZDCF		
		LI		427±7
I	A (97–8); B (98–9)	DCF		414±15
		δ^2	28; 39	417±18
		ZDCF		421±14
		LI		427±11
V	A (96–8); B (97–9)	DCF		432±11
		δ^2	68; 149	429±11
		ZDCF		418±9
		LI		428±14
V	A (97–8); B (98–9)	DCF		433±7
		δ^2	29; 84	432±6
		ZDCF		428±9
		LI		423±3

Table 6. Time delays obtained from the application of a Monte Carlo algorithm with four different methods to the CfA R data

Years	Method	Points (CD)	Delay (CD)	Points (CD-BPF)	Delay (CD-BPF)
A (84–5); B (85–6)	DCF		420±6		419±4
	δ^2	40; 49	420±5	39; 47	421±6
	ZDCF		429±7		428±7
	LI		432±5		431±6
A (85–6); B (86–7)	DCF		419±10		417±12
	δ^2	49; 74	410±13	46; 72	407±15
	ZDCF		420±9		417±12
	LI		409±14		431±8
A (86–7); B (87–8)	DCF		431±12		428±13
	δ^2	53; 58	434±10	52; 58	418±17
	ZDCF		429±15		430±12
	LI		424±9		420±5
A (87–8); B (88–9)	DCF		425±12		428±13
	δ^2	60; 53	423±17	58; 53	422±18
	ZDCF		419±17		411±13
	LI		421±11		422±12
A (88–9); B (89–90)	DCF		417±21		
	δ^2	23; 19	420±10		
	ZDCF		412±8		
	LI		421±2		
A (89–90); B (90–1)	DCF		440±5		424±19
	δ^2	40; 38	407±7	40; 34	420±3
	ZDCF		417±6		420±7
	LI		410±6		411±3
A (90–1); B (91–2)	DCF		435±8		
	δ^2	15; 29	433±18		
	ZDCF		423±19		
	LI		426±6		
A (91–2); B (92–3)	DCF		394±0		394±1
	δ^2	14; 72	402±1	14; 67	403±1
	ZDCF		423±12		416±13
	LI		436±9		437±8
A (92–3); B (93–4)	DCF		411±5		419±6
	δ^2	70; 98	423±2	63; 93	423±2
	ZDCF		411±11		424±15
	LI		423±13		433±3
A (93–4); B (94–5)	DCF		422±4		422±4
	δ^2	83; 111	421±2	78; 95	421±2
	ZDCF		422±6		422±7
	LI		421±4		418±6
A (94–5); B (95–6)	DCF		415±6		418±7
	δ^2	101; 66	411±2	87; 57	415±3
	ZDCF		416±2		416±5
	LI		421±12		418±5

Table 7. Statistical results obtained from the 23 time delays calculated for each method

Method	Mean Delay	Mean Error	Dispersion	r.m.s.
DCF	423.3	10	7	1.4
δ^2	421.8	9	6	1.3
ZDCF	420.6	11	5	1.1
LI	424.3	7	6	1.2
Total	422.6	9	6	0.6

Table 8. As in Table 7 but only considering R filter time delays

Method	Mean Delay	Mean Error	Dispersion	r.m.s.
DCF	423.4	11	6	1.7
δ^2	420.5	8	6	1.7
ZDCF	420.9	11	6	1.4
LI	424.3	8	7	1.7
Total	422.3	10	6	0.8

Table 9. Statistical results obtained only considering time delays and error bars than include part or the whole interval given by the results of Table 6 (420-424 days)

Method	Mean Delay	Mean Error	Dispersion	r.m.s.
DCF	422.2	11	6	1.3
δ^2	421.6	9	6	1.2
ZDCF	420.8	11	5	1.2
LI	423.2	8	4	0.9
Total	422.0	10	5	0.6

Table 10. As in Table 9 but only considering R filter time delays

Method	Mean Delay	Mean Error	Dispersion	r.m.s.
DCF	422.5	11	6	1.6
δ^2	420.9	9	6	1.8
ZDCF	420.9	11	6	1.4
LI	423.0	8	4	1.2
Total	421.7	10	5	0.8